Broadband Simulation of Earthquake Ground Motion by a Spectrum-Matching, Multiple-Pulse Technique

Alexander A. Gusev,[a)] *and Victor M. Pavlov*[b)]

Earthquake Spectra Volume 25, Issue 2, pp. 257-276 (May 2009)

A kinematic, stochastic fault model and simulation procedure is proposed for realistic, application-oriented simulation of earthquake ground motion. An extended fault plane is discretized as a grid of point subsources. Subsource signal, in its low-frequency part, is produced by a dislocation strip sweeping the fault area. In its high-frequency part, it is defined by random local slip history, represented by a segment of pulsed noise. Subsource signals are convolved with broad-band Green functions for a layered half-space, and stacked, resulting in the ground motion at a site. Through a special choice of subsource signals, the Fourier spectrum of ground motion obeys an observation-based scaling law. Effects of the rupture velocity behavior, rise time, wavenumber spectrum for the final slip, the degree of spikiness of time functions etc can be easily analyzed. For illustration, several near-source 1994 Northridge earthquake records are simulated, and related uncertainties are estimated.

INTRODUCTION

Despite many studies that address the simulation of ground motion from a large earthquake, much is still to be done. In general, to simulate earthquake ground motion from a known fault, one should be capable to simulate both (1) fault/source space-time evolution, and (2) wave propagation from the fault to a receiver. The last step may include such separate substeps as (2a) propagation of linear wave up to the bedrock under the site/receiver, and (2b) non-linear propagation in weaker upper layers. We confine our study on (1) and (2a); moreover, in (2a) we use a simple, horizontally layered, model of the Earth's structure.

[a)] Institute of Volcanology and Seismology FEB RAS, 9 Piip Blvd, 683006 Petropavlovsk-Kamchatsky, Russia
[b)] Kamchatka Branch, Geophysical Service RAS, 9 Piip Blvd, 683006 Petropavlovsk-Kamchatsky, Russia

There are two main classes of approaches that have been developed to describe space-time evolution of the earthquake source. The first one is based on the elastodynamic representation of a fault, and treats a fault as a spontaneously propagating crack or dislocation (e.g., Day, 1982). Conceptually this approach is highly attractive, but at present it cannot realistically predict high-frequency (HF) source radiation that defines acceleration amplitudes. In another class of approaches, one uses semi-empirical models that combine some theoretical reasoning with generalization of empirical data. In this line, most important steps are: the concept of approximate self-similarity of earthquake source process that implies a spectral scaling law (Haskell, 1966; Aki, 1967); the particular omega-square spectral scaling law with self-similarity (Aki, 1967; Brune, 1970); demonstration of lack of self-similarity in actual broadband spectral scaling (Gusev, 1983); derivation of properties and parameters of strong motion based on spectral scaling law, both assuming similarity and using point source model (Hanks and McGuire1981), and suggestion of broadband semi-empirical finite source models with no spectral similarity (Gusev, 1983; Papageorgiou and Aki, 1983). In numerous studies, the source of a large earthquake was represented as a composition of earthquake sources of smaller size (e.g., Boatwright, 1982, Papageorgiou and Aki, 1983). For fault-to-site distances comparable or exceeding fault size, approaches of this second class have produced some quite useful techniques for broad-band ground motion simulation (e.g. Hartzell et al. 1999). However, most of these approaches lose their efficiency if one needs to predict the ground motion at small distances where emulation of finer details of space-time evolution of a large event becomes critical.

In a broadband simulation of an earthquake source, one should comply simultaneously with the following two critical requirements: (1) the low-frequency component of simulated signal must incorporate our understanding of details of real fault propagation, first of all the running strip model of Heaton (1990) and final slip structure conjectured by Andrews (1980) based on the fractal concept, and then confirmed by geological (Yin and Ranalli (1995) and seismological (Tsai 1997) evidence; and (2) the high-frequency component has to comply with our empirical knowledge of typical Fourier spectra at moderate-to-large distances, and also to emulate spikiness (non-Gaussian heavy-tailed amplitude statistics) of observed near-fault accelerograms (Gusev, 1996). Until the elastodynamical models mature to fulfill these requirements, kinematic (phenomenological) models can be developed to meet the demands of engineering applications. The approach presented below is of the second kind; it is aimed

to satisfy the listed requirements ignoring dynamic evolution of a propagating fault but incorporating observational knowledge of fault behavior.

There is one important difference between elastodynamic models incorporating crack tip motion, and the present approach; it regards the directivity of HF radiation. At typical rupture velocities, with v_{rupture} / v_S above 0.6, crack tip motion can create significant HF directivity; but this effect is rarely observed in data. In the present model, HF directivity of this kind does not exist; there is a limited directivity however, related to direction-dependent duration of source time function.

In our approach, the source simulation is done in two steps. First we generate a preliminary model that emulates such critical details as low-frequency behavior, high-frequency envelope structure and statistics of peaks. However, this model would produce unrealistic, nearly-white-noise displacement signal. Therefore we then smooth the source signal in an accurately controllable manner, fitting an empirical spectral scaling law.

The presented simulation procedure is aimed at a realistic prediction of earthquake ground motion for the magnitude range Mw 5 to9, the distance range from 5-10 to 200-300 km and frequency band 0-25 Hz. The earthquake source is represented as a grid of point sources with appropriate time histories. For any site in question, and for each subsource, we calculate the response of layered medium to a unit step in seismic moment for a point dislocation (Green function) and convolve it with the respective time history. Such contributions of all subsources are added up, to result in a synthetic ground motion. Correspondingly, the entire simulator procedure consists of the following modules: (1) source simulator, (2) Green function calculator, and (3) convolver-summator. We use an original Green function calculator for layered medium, accurate over the entire relevant frequency band, from static terms (producing the “swing” motion) to rather high frequencies. To illustrate capabilities of the proposed method we simulate near-source ground motion of a well-recorded earthquake, making minimal parameter adjustments (nearly “blind test”). As the specification of uncertainty of the simulated ground motions is a highly important component of engineering-oriented simulation, we also make example of uncertainty analysis, taking the already performed simulation case as a reference case.

The present text is a compressed version of the preliminary one (Gusev and Pavlov 2006) that contains many significant details, in particular regarding the analysis of uncertainty.

THE TECHNIQUE FOR THE SIMULATION OF STRONG GROUND MOTION

SOURCE SIMULATOR

The source simulator algorithm is based on the generalized version of the classic Haskell (1966) stochastic fault model that assumes that at a particular point of a fault, the process of slip formation is of definite duration, denoted "rise time", much smaller than rupture propagation time. Haskell also proposed that the fault slip rate is a random function of time. We follow these two assumptions, and introduce the following modifications:

1. Instead of the Haskell's fault with a constant final slip, a variable, random final slip is assumed, governed by power spectrum that is a power law with respect to wavenumber (Andrews 1980; Yin and Ranalli 1995; Tsai 1997; and later work). With respect to amplitude statistics, random slip function is assumed to be heavy-tailed, and simulated so as to be log-normally distributed, with coefficient of variation CV_{xy}.

2. Kinematics of a Haskell's source is generalized in the following way: the rupture front is of a general shape (not a straight line); the nucleation point is arbitrary; and the rupture velocity is not a constant but a random function over the fault area with a prescribed mean.

3. Instead of the Haskell's "omega-cube" far field spectrum, the far-field spectrum of a simulated source is constructed so as to approximate, in its high-frequency part, the particular "target" spectral shape derived from a preset regional spectral scaling law.

This general concept is to be realized in a numerical scheme. Following in many respects the incoherent source representation of Gusev (1983) we introduce a grid of point-like dislocation subsources with uncorrelated time histories. Each subsource represents a particular cell of the grid. It possesses a certain fraction of the total seismic moment, and the distribution of seismic moment over subsources is governed by the aforementioned random final slip function. The size of a subsource is selected based on a tradeoff between the desire to keep the total number of subsources within some limits, and the intention to perform the signal synthesis near to the fault with certain fidelity. Let r be the shortest distance from a station to the surface of the fault. We believe that for the simulation to be physically meaningful, at least several point subsources must be located within in the distance range of about (1-2)r. To fulfill this requirement, the size of a subsource d (equal to the cell size of the subsource grid), must be significantly smaller than r; a practical constraint can be set as $d<0.3r$. The program was tested successfully with as many as $40\times20=800$ subsources. Let us

consider this particular grid, and determine lower limit of acceptable r values, r_{min}, for a set of magnitudes. For M_w=[6.5, 7.5, 8.5], the 40×20 grid corresponds to d values of about [0.6, 2, 6] km; this leads to r_{min}=[2, 7, 20] km, correspondingly. At large distances, a limited number of subsources can be sufficient for acceptable representation of ground motion; however grids smaller than 13×3 cannot be recommended.

The duration of a subsource is defined by the value of rise time T_{rise} (the duration of local slip), assumed the same over the entire fault in the current version of the algorithm. However, a technical problem may arise when T_{rise} is smaller then duration of a pulse that would be recorded from a finite subsource with delta-like time function; this duration is of the order $T_{fiit} \approx d/v_S$. In such a case, pulses from individual subsources do not overlap smoothly, and artifacts can appear on synthetic traces in the form of individual bursts of displacement or HF energy. The need to avoid this problem adds one more constraint on the size of a subsource: it must be smaller than $v_S\, T_{rise}$. (Alternatively, the value of T_{rise} can be artificially increased.)

Each subsource has an individual, random moment rate time history. In absolute time, subsources are switched on by the arrival of the rupture front; otherwise their time histories are uncorrelated ("incoherent source" see Gusev (1983)). In the present model, individual point subsources bear no direct physical meaning; they serve only as a tool for numerical simulation. Thus, their correlation properties must match the correlation properties of slip rate function in space and time, and these properties are poorly known. One can expect however that for small adjacent fault patches, some correlation between their slip rate time histories must arise. Therefore, the assumption of complete incoherence becomes inadequate for a dense subsource grid. This is an additional reason not to use very large grids, and thus not to apply the present technique too near to a fault.

The above considerations led us to the simulation procedure with the following steps:

1. **Specification of parameters of the model.** These include common source parameters like seismic moment, strike, dip and rake angles, stress drop $\Delta\sigma$, nucleation point position, rise time and mean rupture velocity v_{mp}. The fault shape is assumed to be rectangular, length L × width W. The values of L and W can be either preset, or calculated from adjustable $L(M_{w,}\, \Delta\sigma)$ and $W(M_{w,}\, \Delta\sigma)$ correlation relationships. Also, parameters of the numerical model are set, namely: the subsource numbers along L and W, and time step.

2. **Monte-Carlo simulation of the final slip distribution.** This simulation begins with generating 2D random white Gaussian spectrum that represents logarithm of slip in wavenumber domain. Then isotropic power-law filter is applied; its exponent *s* is preset. The result is Fourier transformed to coordinate domain, and rescaled so that its rms deviation becomes equal to the certain preset value, CV_{xy}. Then, the obtained function is exponentiated, resulting in positive random function with lognormally distributed values. This function represents a piece of stationary 2D random field. To emulate slip function over a limited *L* by *W* rectangle, it is multiplied by 2D taper ("cap") function, equal to zero outside the rectangle. If a side of a fault cuts the free surface, tapering is switched off along it. Tapering somewhat distorts the initial power-law spectral shape; this kind of distortion is inevitable for a function defined on a limited area of a plane, and thus is tolerated. The value of CV_{xy} defines how heavy-tailed shall be the distribution of values of the simulated final slip. Technically, CV_{xy} equals, approximately, to the coefficient of variation for amplitudes; this explains the notation. Note that the existence of "asperities", or patches of expressedly high fault slip, is an alternative way to say that fault slip bears heavy-tailed statistics. Therefore, the value CV_{xy} controls how sharp and expressed are "asperities". See Fig. 1 for an example of simulated final slip. Selection of particularly lognormal distribution was originally a guess, based on its following useful properties: it produces non-negative values, and by appropriate choice of CV_{xy} it can either be easily adjusted to express almost any practically required degree of non-Gaussian behavior, or made to approximate the Gaussian law. Recently, lognormal distribution was also found to describe reasonably the results of several inversions of slip in earthquake faults (to be published elsewhere).

3. **Monte-Carlo simulation of the rupture propagation history.** First of all, the fault-average value v_m of rupture velocity is determined. In the primitive mode, it equals v_{mp} . In a more advanced mode, v_{mp} is treated as the mean value for a fault population; to determine the value of v_m for an individual fault, v_{mp} is perturbed by uniformly distributed random term, with zero mean and half-range dv_r. The rupture front is assumed to form a circle centered at the nucleation point; it moves in steps of identical length, smaller than the size of a subsource cell. At the *i*-th step, the value v_i of local/instant rupture velocity is determined as a product of the constant value v_m, and of a random number drawn from uniform distribution in the range (1-*DV*, 1+ *DV*), where *DV* is another preset parameter. Alternatively, the front propagation history can be controlled by 2D distribution of random values of rupture velocity. For an example of simulated rupture front propagation see Fig. 1.

4**. Monte-Carlo simulation of preformed time histories for subsources.** For each subsource, its preformed time history is a provisional version of its moment rate function. Conceptually, this time history was intended to represent a sequence of positive delta-like pulses (spikes) with random delays and amplitudes that are caused by failure of local strong spots ("mini"-asperities, like those introduced in (Gusev 1989)) within the subsource area. Correspondingly, the subsource time history can be represented by a segment of modulated positive white noise, with duration defined by T_{rise}. The integral of noise amplitudes equals to the seismic moment of the subsource. The simplest shape function for the modulating envelope is boxcar of duration T_{rise}, there are other options for the shape function as well. The amplitude statistics of noise is again assumed lognormal, with (logarithmic) variance parameter CV_t^2. Technically, CV_t is close to the coefficient of variation for spike amplitudes. By adjusting CV_t, one can define whether the resulting accelerograms will appear like Gaussian noise or will look spiky to a certain controllable degree. For each subsource, the onset time of a sequence is determined by the arrival time of the rupture front to its position. The simulated amplitude statistics of spikes is intended to emulate heavy-tailed, non-Gaussian statistics of acceleration peaks (Gusev 1996). The complete set of preformed time histories of subsources represents a "preformed source". For illustration see Fig. 1 and 2.

5. **Creating the "finishing operator".** At this point, the preliminary source description has already been constructed, with realistically set low-frequency behavior, envelope shape and peak statistics of its HF component. The only remaining problem is the unrealistically high level of spectral amplitudes at high frequencies, i.e., above (4-6)×(corner frequency). To rectify this deficiency, we modify the preformed time functions through application of a specially designed "finishing operator". In time domain, it reduces to smoothing, performed through convolution with a certain positive pulse ("finishing pulse"). Integral of this pulse is set to unity, to guarantee that the M_0 value of the preliminary source will be kept unchanged. The finishing operator is constructed in frequency domain, in the following way. First, we calculate the source spectrum (Fourier spectrum of the moment rate time history of an equivalent point source) $\dot{M}_0^{(PRF)}(f)$ that corresponds to the time history of the preformed source, obtained by stacking all subsources. We then compare the result with the preset "target" source spectrum $\dot{M}_0^{(PRF)}(f)$, derived from the regional spectrum scaling law for the given values of moment magnitude and stress drop (that is, ultimately, from averaged observed strong motion spectra). We calculate the ratio of these two spectra, and smooth it by

Gaussian window. The result is then modified: it is set to unity at frequencies below $0.2f_c$, so as not to distort low-frequency part of the spectrum which is already acceptable. In this way we obtain the module of the "finishing operator" in frequency domain. Its phase spectrum is adjusted so as to make its time-domain representation causal (minimum-phase). This procedure is illustrated on Fig. 3. Finishing operator is shown in frequency domain on Fig.3b, and in time domain, ("finishing pulse"), on Fig. 3d, marked D on both graphs; it converts $\dot{M}_0^{(PRF)}(f)$ to final source spectrum $\dot{M}(f)$. Operators marked V and A can be used to convert $\dot{M}_0^{(PRF)}(f)$ to $\ddot{M}_0(f)$ and $\dddot{M}_0(f)$.

6**. "Finishing".** The "finishing" procedure, i.e., smoothing by convolution with "finishing pulse", is applied to preformed time histories of each subsource, giving a final version of its time history of subsources. The spectrum of their sum, in its high-frequency part, approximates the "target" spectrum in the rms sense. In time domain, the same sum gives the shape of the far-field body wave displacement signal for a ray normal to the fault. Similarly, using for convolution first and second derivatives of the finishing pulse (Fig. 3), one obtains the shapes of far-field velocity and acceleration signals, as illustrated in Fig. 1 for an individual subsource.

The described source simulation algorithm is capable of producing realistically-looking far-field and near-field ground motions. In particular, it reproduces well the common directivity effects for the velocity pulse, but do not create unrealistically high directivity for HF (acceleration) signal. Also, it successfully emulates, in terms of amplitude levels, observed peak accelerations and velocities, as well as response spectra and characteristic durations.

These results are, in a sense, too good however because the described procedure reproduces average spectra and amplitudes with unnaturally low scatter, "too accurately". This fact results from the feedback loop inherent within the described procedure: the simulated *individual* spectrum reproduces the fixed target spectrum too precisely, and the natural variability of signals is strongly dampened. This property may be considered as an advantage if one needs a single representative example of future strong motion. But from a geophysical viewpoint, as well as from the viewpoint of probabilistic properties of a suite of simulated ground motions, this is a deficiency. The case shown in Fig. 3 was generated just in the described mode; the resulting too perfect spectral fit can be noticed in Fig 3c.

To make amplitudes and response spectral levels fluctuate realistically from one simulation run to another we must disjoin the mentioned feedback loop, thus increasing the purely-random variability of ground motion up to the correct level, whereas not perturbing the *average* amplitude and spectral levels. Towards this end, a special procedure was constructed (to be presented elsewhere) that increases the scatter of spectra of an individual simulation run around the average (over many simulations) spectrum; the resulting degree of scatter corresponds to the level expected from the random vibration theory. After such a modification, the algorithm generates signals with realistic variability. Only these are adequate for such uses as generating suites of design earthquake ground motion, and/or analyzing variability/ uncertainty of the results. In some special cases, when we wish to generate a single "typical" ground motion, or to evaluate the sensitivity of results to variations of input parameters of the model, we do not use this procedure.

GREEN FUNCTION CALCULATION AND CONVOLUTION

To match the level of accuracy promised by the source simulator described above, an accurate broadband Green function calculator was needed. We use the original discrete wavenumber code that calculates pulse response of the layered elastic medium to a step-like point double-couple source. The code is based on the advanced version of the method of Alekseev and Mikhailenko (1980), developed recently by Pavlov (2002, 2009). The solution is initially represented in cylindrical coordinates as an integral sum over surface vector harmonics. Alekseev and Mikhailenko (1980) introduce a distant boundary and convert the integral representation into a series over discrete wavenumbers that are roots of a certain equation related to Bessel functions. To determine coefficients of this series, for each frequency-wavenumber pair one must solve ordinary differential equations in depth coordinate (a single equation for the SH case and a pair of coupled equations for the P-SV case). These differential equations are solved analytically, layer by layer, introducing the impedance matrix (relating stress vector to motion vector) and the motion propagator matrix (connecting motion vectors on two boundaries). For SH waves in particular, impedance is the scalar function of depth such that the stress component is equal to the product of the impedance and of the motion component. For the P-SV case, impedance is introduced in a similar way, forming a 2×2 matrix. The impedances and the motion propagators are calculated by closed analytical formulas. The advantage of the presented method is that it is numerically stable, in contrast to conventional propagator methods (where propagator

connects stress-motion vectors). This is because in our method, all relevant exponential factors are below unity by absolute value. To ensure the preset level of numerical accuracy in a uniform way, the number of terms in the series expansion is selected adaptively. The developed numerical method provides an accurate broad-band representation of ground motions in a layered medium. It has no intrinsic limitations with respect to bandwidth, and predicts both so named "swing effect" at zero frequency, and high-frequency body wave spikes equally well.

In the convolution module, for each site, the first step is to convolve over time the subsource time histories and the corresponding Green functions. The second step is to add thus obtained contributions of all subsources, resulting in the ground motion at the site.

Intrinsic loss can be accounted for in two ways: either as a spectral correction, through κ(kappa) factor (generally, distance-dependent), with assumedly depth-independent Q, or through a frequency-independent vertical Q profile included within the Green function calculation.

The present version of Green function calculator does not incorporate scattering of HF waves; it therefore needs further improvement to emulate reliably strong motions at distances of 70-100 km and more.

PARAMETERS OF THE MODEL

We list below the parameters that define a particular realization of our numerical model. Parameters can be selected/modified to attain such aims as: (1) tuning both the source model and the model of the medium to a particular seismological situation, by setting appropriate particular values of parameters; (2) analyzing the variability and uncertainty of the predicted motion, both purely random and parameter-related; and (3) generation of a suite of representative ground motions. We list the most important parameters of the model.

A. Parameters of earthquake source/fault and of regional seismicity.

1. General.

1.1. Geographic coordinates φ_c, λ_c and depth H_c for the center of the fault rectangle .

1.2. Moment magnitude M_w.; strike, dip and rake angles.

1.3. Stress drop parameter δ, defined as logarithmic deviation of individual stress drop value from its regional average ($\delta=\Delta\log_{10}\Delta\sigma$).

1.4. Length L and width W of the fault rectangle; numbers of subsources: n_L along L and n_W along W

2. Kinematics and dynamics.

2.1. CV_{xy}: defines how spiky/non-Gaussian will be the simulated final slip function.

2.2. The exponent s in the power law defining the power spectrum ($\propto k^{-s}$) of the final slip.

2.3. Location of the nucleation point (x_n, y_n along L and W, or φ_n, λ_n and H_n).

2.4. Parameters of rupture velocity distribution: fault population mean value v_{mp}, half-range dv_r of dispersion for the average value of velocity v_m for an individual fault, relative range DV of random perturbation (with respect to v_m) of instant/local value of rupture velocity at a particular spot of an individual fault). Note that our "rupture velocity" is a smoothed entity like in (Papageorgiou and Aki 1983), and not a local crack tip velocity.

2.5. Rise time T_{rise}

2.6. CV_t : defines the degree of non-Gaussian behavoir ("spikyness") of accelrograms.

3. Random seeds

3.1. Random seed defining the final slip function.

3.2. Random seed defining the time histories of subsources.

3.3. Random seed defining the perturbation of the mean value of rupture velocity.

3.4. Random seed defining the random history of rupture velocity

3.5. Random seed defining the perturbation of the nucleation point position.

4. A particular average regional scaling law for source spectra $\dot{M}_{0ref}(f \mid M_w)$ or

$\dot{M}_{0ref}(f \mid M_0)$, as a table or formula, for a certain reference stress drop value, $\Delta\sigma_{ref}$.

B. Parameters of the layered medium and of a site: (1) the site position; (2) the velocity-density column for a site (includes depth to the top of a layer, ρ, V_P, V_S,) and (3) intrinsic loss specification, either through Q_P and Q_S for each layer, or through κ for a site, and $Q(f)$ vs. distance.

For a given, arbitrary value $\Delta\sigma$ of stress drop, target spectra cannot be simply extracted from the empirical regional spectral scaling law. To modify them correspondingly, we use the parameter $\delta=\Delta\log_{10}\Delta\sigma=\log_{10}(\Delta\sigma/\Delta\sigma_{ref})$. It is introduced in order to simplify the simulation when different researchers use different definitions and techniques to introduce and determine $\Delta\sigma$ values. Of course, $\Delta\sigma$ and $\Delta\sigma_{ref}$, when used, must be defined identically, or

determined by similar techniques. The use of δ parameter permits one to manage also without the knowledge of actual values both of $\Delta\sigma$ for a target event or $\Delta\sigma_{ref}$ for a regional average spectral law. The value of δ can e.g. be estimated from the deviation of the fault area of the target event from the regional trend, or from similar deviation of the m_b:M_w ratio, and so on. With the value of δ at hand, the reference empirical spectral shape is modified in the following way (as proposed by G. Panza (personal communication, 1999)).

$$\dot{M}_0^{(TAR)}(f \mid M_0, \delta) = 10^{\delta} \dot{M}_{0ref}(f \mid M_0 10^{-\delta})$$

In the present version of the algorithm, several particular spectral scaling laws are preset: (1) for W.USA shallow earthquakes, following Joyner's (1984) modification of Brune's (1970) scaling law (assuming similarity); (2) semi-empirical scaling law of Gusev (1983), with no similarity, and more.

AN EXAMPLE CASE: NORTHRIGE 1994 EARTHQUAKE

An appropriate test for the algorithm described above is its application for the emulation of a set of records obtained in the epicentral zone of a large earthquake on various ground types. To perform such a test, 19 near-source records of M=6.7, 1994, Northridge, California, earthquake were simulated (see Fig. 4 for the general overview). We tried to perform the simulation with minimal of fitting, as near to a "blind test" as possible. Most of source parameters used in our simulation are adapted from (Wald et al, 1996), other parameters were fixed in an a priori manner. See Table 1 and comments under it. We employ a scaling law for source spectra from Joyner (1984), combined with kappa filter ($\exp(-\pi\kappa f)$) according to Anderson and Hough (1984). The only parameter whose values were fit to real data is the κ parameter of this filter.

The vertical velocity-density profiles for stations (Table 2) were selected in the following way. For stations whose ground was specified as "rock" and "deep soil"/"basin", profiles indicated as "rock" and "soil" geology were borrowed from Wald et al.(1996). The velocity profile for "stiff soil" stations in Table 2 was selected as approximately intermediate between "rock" and "soil" profiles of Wald et al.(1996), these stations called "intermediate" in the following. The complete list of stations is included in Table 2; detailed station/record data can be obtained from http://peer.berkeley.edu/smcat/.

Only local attenuation (kappa factor) was taken into account in this simulation; distance-dependent term was omitted. The values of κ, determined by trial and error, are equal to 0.04, 0.05 and 0.075 s for rock, intermediate and soil stations, respectively. Among them, the value 0.075 s for soil/basin may look unusually large; actually, this value correctly reflects significant non-linear enhancement of attenuation in a soft soil in the epicentral zone, see e.g., Hartzell (1998).

Two examples of simulation, #206 and #300, were selected for demonstration out of ten variants generated in ten successive runs of the code. To generate these variants, we changed independently three random seeds that define: 2D final slip function, subsource time functions, and rupture front time history, respectively. In the two selected variants, ground motion parameters are quite comparable to the observed ones. On Fig. 4 we show moment rate functions for subsources for variant #206. On Fig. 5 one can see the combined far-field signals from entire source for both variants. On Fig 6 we compare simulated and observed time histories of ground motion at five representative stations for variant #206. The general appearance and amplitudes match acceptably; however, the observed motion at rock stations is somewhat more spiky (non-Gaussian) than the simulated one.

Let us now discuss the numerical differences between simulated and observed time functions. (Simulated functions were rotated and filtered to match the recorded ones). We analyze these differences in the form of logarithmic amplitude misfit, denoted generally as $\Delta\log_{10}(A)= \log_{10}(A(\text{simulated}) - \log_{10}(A(\text{observed}))$. The misfit was determined for pseudo response acceleration PRA ($\Delta\log_{10}(\text{PRA})$) calculated over 25 frequencies between 0.1 and 20 Hz, and also for the peaks of acceleration, velocity and displacement, and averaged over the two horizontal components and over 19 stations. On Fig. 7, one can see $\Delta\log_{10}(A)$ for the two (#206 and #300) variants out of 10 simulated. The visible deviations from the ideal fit (that would give a horizontal line) are thought to demonstrate a real tendency of ruptures on the same fault neither to copy one another, nor to reproduce accurately any regional scaling law. The average misfit over 10 variants and 25 frequencies is less than 0.03 in $\log_{10}$ units (7% in A); and rms deviations of amplitude residuals among stations are about 0.17 $\log_{10}$ units. On the whole, the results of comparison can be considered as quite satisfactory. Bazzurro et al.(2004) studied how well the results of seven different techniques for simulation of ground motion, including one presented here, can simulate linear and especially non-linear response of a single-degree-of-freedom system to the observed motion of the 1994 Northridge

earthquake. The technique described above was the only one that produced realistic results over the entire frequency band analyzed (0.25-10 Hz).

UNCERTAINTY ANALYSIS

The developed simulation technique was also applied to the estimation of uncertainty of the predicted ground motion for the 1994 Northridge earthquake at the same 19 stations. Random variability related to intrinsically stochastic part of the model is simulated by using a series of sets of random seeds. To deal with random variability related to the natural variability of input parameters, we suppose that the distribution of an input parameter, (e.g., "*x*"), is known, and derive distribution of an output parameter (e.g., "*y*"), using sensitivity (i.e., derivative *dy/dx*). Three groups of factors were analyzed: random seeds, parameters intrinsic for the fault, and external parameters. To simplify the tabulation of results, all individual factors contributing to uncertainty were enumerated; these numbers serve as item numbers in the list below.

The uncertainty related to first group – random seeds - was analyzed directly in terms of rms deviation σ_{log} of the individual $\log_{10}(A)$ values obtained in 16 successive tries. The factors whose effect was studied were:

(1) random seed defining the final slip distribution over the fault;

(2) random seed defining subsource time histories;

(3) random seed defining random variations of instant rupture velocity over the fault area;

(4) the random value of mean rupture velocity, considered to be distributed uniformly within the range 2.16-3.24 km/s (Mach number v_m/v_S=0.6-0.9); and

(5) the random position of nucleation point, considered to be distributed uniformly over the lower third of the fault area. Note that although the latter assumption seems to be reasonable in the particular case under study, it significantly suppresses the dispersion of results caused by variations in directivity.

Six parametric source-related factors were analyzed using sensitivity approach. In the list of factors, for each item, we give *in brackets* the value of sensitivity ($d\log_{10}(A)/d$(parameter)) that has been estimated in our analysis. For the lack of space, we cite only averages over all 25 analyzed frequencies. In cases of expressed non-linearity, minimal estimate is taken. The assumed rms deviation of a parameter is then listed *in braces*.

(6) Stress drop $\Delta\sigma$. During variation of $\Delta\sigma$, fault center was fixed. [$d\log_{10}(A)/d(\log_{10}\Delta\sigma)$=0.32]{0.1}.

(7) Coefficient of variation CV_t for amplitudes of preformed subsource time function. [0.19]{0.15}.

(8) Coefficient of variation CV_{xy} for the values of final slip distribution. [0.091]{0.15}.

(9) The range of variations for the rupture velocity *DV*. No clear effect was noted for the studied range *DV* =0.0 - 1.0; probably the assumed range for *DV* is unrealistically small.

(10) Effect of the exponent *s* in the power law for the power spectrum of the final slip. No clear effect was noted for the studied range *s* =1.0-2.2.

A few more factors were included that are external to the source; their analysis is much less interesting because their effect strongly depends on the particular geometry of the fault and of the station set, and thus is of low generality. Among these factors, only dip angle and H_c were found to be significant.

(11) Dip angle, degrees. [0.024]{10º}.

(12) H_c, km. [0.045]{2.5}.

For factors 6-12, σ_{log} was determined as the product of sensitivity and assumed rms deviation of a factor. The uncertainty related to variable station geology was estimated empirically from inter-station standard deviation of $\log_{10}(A)$. The uncertainty related to deviations of the actual source spectrum from a regional average spectral scaling law was ignored. The uncertainty produced by unreliable value of seismic moment can be estimated from theoretical considerations: for the LF range, sensitivity $d\log_{10}(A)/d\log_{10}(M_0)$ equals 0.5-0.67; for the HF range: $d\log_{10}(A)/d\log_{10}(M_0)$ = 0.2-0.3. Effects of this factor were not included into further calculations.

The results are listed in Table 3, for PSA averaged over various frequency bands, and for peak amplitudes. Rows of this table are denoted: (1) for PSA: average value over all frequencies is denoted as “A”; averged over 0.1 to 0.3 Hz band as “XL”; similarly for 0.31 to 1.5 Hz: “L”; 1for .51-5 Hz: “M”; and for 5.1-20 Hz: “S”); (2)for peak acceleration:“a”, for peak velocity: “v”, and for peak displacement:“d”. In the header line numbers of factors are given, as specified above. The S_f column lists joint rms deviation calculated assuming independence of effects of the analyzed factors; this assumption seems to be reasonable in the

case analyzed. The column S_{is} lists interstation rms deviation of amplitudes in a particular simulation variant, averaged over ten such variants. These values give an empirical estimate of uncertainty related to a "random" selection of a site among sites of a certain (definite) ground type. The column S_{tot} is obtained through summation of variances related to columns S_f and S_{is}, it gives our estimate of total uncertainty. Note that all the analyses above are based on rms averages of *A* values of two horizontal components.

Short comments can be given here regarding the results in Table 3. The station term contribution to uncertainty is relatively large, reflecting variations in site geology, path effects and maybe unaccounted directivity effects. Among other factors, random seeds and parametric factors contribute approximately equally. Among random seeds, the effect of variation in fault-average rupture velocity is the largest. Note that we assumed minimum uncertainty for parameters, thus the estimates of Table 3 must be treated as "less conservative".

CONCLUSION

In the development of the proposed broad-band simulation procedure it was planned to incorporate most well-established properties of earthquake sources. The resulting procedure, though judging by a single test only, is quite attractive: in the mode of almost blind testing, the match to observations in the epicentral zone is quite satisfactory. Another attractive result is the demonstrated possibility to generate uncertainty estimates; this capability is inportant for any engineering-oriented application. More work is needed to verify wider applicability of the proposed technique. Also, recommendations must be elaborated for the choice of a few parameters of the source model whose values are no more than guessed at present.

ACKNOWLEDGEMENTS

The work was supported by the SAND group of the Abdus Salam International Center for Theoretical Physics, Trieste, Italy and by the Russian Foundation for Basic Research (grant 07-05-00775). Authors are indebted to Giuliano Panza who proposed the study. Discussions with him, Fabio Romanelli and Franco Vaccari were highly valuable. The analysis of uncertainty was proposed by the Organizing Committee for Treasure Island prediction exercise; they also kindly provided preprocessed observational data. Comments of anonymous reviewers were helpful in improving the manuscript.

REFERENCES

Aki, K. 1967. Scaling law of seismic spectrum: *J. Geophys. Res*. **72**, 1217-1231.

Alekseev A.S, Mikhailenko B.G. 1980. The solution of dynamic problems of elastic wave propagation in inhomogeneous media by a combination of partial separation of variables and finite-difference method. *J. Geophys.* **48**, 161-172.

Anderson J.G. and S.E. Hough, (1984) A model for the shape of the Fourier amplitude spectrum of acceleration at high frequencies, *Bull. Seismol. Soc. Am.,*74, 1969-1993.

Andrews, D. J. 1980. A stochastic fault model. 1. Static Case. *J. Geophys. Res*., **78**, 3867-3877.

Bazzurro, P., Sjoberg, B., and Luco, N. 2004. Post-Elastic Response of Structures to Synthetic Ground Motions, Tech. Rep. AT2, PEER Lifelines Program 1G00, AIR Worldwide Co., San Francisco.

Boatwright, J. 1982. A dynamic model for far-field acceleration, *Bull.Seism. Soc. Am.* **72,** 1049–1068.

Brune, J. N. 1970. Tectonic stress and the spectra of seismic shear waves from earthquakes, *J. Geophys. Res.* **75**, 4997–5009.

Day, S.M. 1982. Three-dimensional simulation of spontaneous rupture: the effect of nonuniform prestress, *Bull. Seism. Soc. Am.*, **72**, 1881-1902.

Gusev A.A. 1983. Descriptive statistical model of earthquake source radiation and its application to an estimation of short-period strong motion. *Geophys. J. Roy. Astr. Soc.,* **74,** 787-808.

Gusev A.A. 1989. Multiasperity fault model and the nature of short-period subsources. *Pure Appl. Geophys*., **130**, 635-660.

Gusev, A.A. 1996. Peak factors of Mexican accelerograms: evidence of non-Gaussian amplitude distribution. *J. Geophys. Res*. **101**, 20083-20090.

Gusev A.A. and V.M. Pavlov. 2006. Wideband simulation of earthquake ground motion by a spectrum-matching, multiple-pulse technique. Trieste, Intl. Centre Theor. Phys., Preprint IC2006023, 27pp. (URL: http://users.ictp.it/~pub_off/preprints-sources/2006/IC2006023P.pdf)

Hanks, T. C., and R. K. McGuire. 1981. The character of high-frequency strong ground motion, *Bull. Seism. Soc. Am.* **71**, 2071–2095.

Hartzell, S., S. Harmsen, A. Frankel, and S. Larsen. 1999. Calculation of broadband time histories of ground motion: Comparison of methods and validation using strong-ground motion from the 1994 Northridge earthquake, *Bull. Seism. Soc. Am*. **89**, 1484-1504.

Hartzell, S. 1998. Variability in nonlinear sediment response during the 1994 Northridge, California, earthquake. *Bull. Seism. Soc. Am*. **88**, 1426-1437.

Heaton, T.H., 1990. Evidence for and implications of self-healing pulses of slip in earthquake rupture. *Phys. Earth Planet. Inter.*, **64**: 1-20.

Haskell, N.A., 1966. Total energy and energy spectral density of elastic wave radiation from propagating faults. II. A stochastic fault model. *Bull. Seism. Soc. Am.*, **56**, 125-140..

Joyner, W.B., 1984. A scaling law for the spectra of large earthquakes, *Bull. Seism. Soc. Am.*, **74**, 1167-1188.

Papageorgiou A.S. and Aki K., 1983. A specific barrier model for the quantitative description of inhomogeneous faulting and the prediction of the strong ground motion. I. Description of the model, *Bull. Seismol. Soc. Am.*, **73**, 693-722.

Pavlov V.M. 2002. A convenient technique for calculating synthetic seismograms in a layered half-space. *Proceedings of the 4th International Conference "Problems of Geocosmos",* St-Petersburg, pp. 320-323. (In Russian).

Pavlov V.M. 2009. Matrix impedance in the problem of calculation of synthetic seismograms in a uniformly layered isotropic elastic medium. *Fizika Zemli*, in press. (In Russian, with parallel English edition).

Tsai C.-C. P. 1997. Slip, stress drop and ground motion of earthquakes: a view from the perspective of fractional Brownian motion. *Pure Appl.Geophys*. **149** 689–706.

Wald D.J., Heaton T.H, Hudhut K.W. 1996. The slip history of the 1994 Northridge, California, earthquake determined from strong ground motion, teleseismic, GPS, and leveling data, *Bull. Seism. Soc. Am.*, **86**, S49-S70.

Yin Z.-M., and Ranalli G. 1995, Modeling of earthquake rupturing as a stochastic-process and estimation of its distribution function from earthquake observations *Geophys. J. Int.,* **123,** 838-848.

Table 1. Assumed values for fault parameters that were used for simulation

φ_c	λ_c	H_c	Strike	dip	rake	M_w	L	W	n_L	n_W
34.28°	-118.56°	12.5 km	122°	40°	101°	6.7	18 km	24 km	7	7

v_{mp}	T_{rise}	φ_n	λ_n	H_n	δ^*	DV^{**}	CV_t^{***}	$CV_{xy}^{\#}$	$s^{\#\#}$
3 km/s	0.7 s	34.35°	-118.54°	17 km	0.15	0.8	0.5	0.5	1.5

* δ=0.15 means that stress drop $\Delta\sigma$ is 1.4 times above the regional average: compare the value of Wald et al (1996), ($\Delta\sigma$=74 bar) to the reference value of 50 bar of the Brune-Joyner spectral model.

** An assumption; our results suggest that it is probably too low.

*** A tentative value based on our experience with simulation, a trade-off between approximately Gaussian accelerograms and expressedly non-Gaussian traces with seemingly too prominent individual spikes.

A similar tradeoff between nearly-constant slip at CV_{xy}=0-0.2 and too prominent asperities at CV_{xy}>0.8.

Andrews'(1980) proposed s=2 as a reasonable assumption; empirical estimates are 1.1-1.3 (Yin and Ranalli 1995), and about 1.7 (Tsai 1997 and later work). We chose an intermediate value.

Table 2. Vertical velocity-density profiles

Layer top depth, km	**Vp, km/s**	**Vs, km/s**	**Density, t/m^3**
"Rock" profile (rock to soft rock: LA0, LDM, PAC, SSU)			
0.0	**1.9**	**1.0**	**2.1**
"Soil" profile (Deep soil/basin: ARL, CNP, JEN, NWH, WPI, STC, PAR, RRS, SPV, RO3, SCS, SCE, SYL)			
0.0	**0.8**	**0.3**	**1.7**
0.1	**1.2**	**0.5**	**1.8**
0.3	**1.9**	**1.0**	**2.1**
"Intermediate" profile (Shallow stiff soil: PKC, KAT)			
0.0	**1.2**	**0.5**	**1.8**
0.1	**1.9**	**1.0**	**2.1**
0.3	**3.8**	**1.5**	**2.2**
all profiles			
0.5	**4.0**	**2.0**	**2.4**
1.5	**5.5**	**3.2**	**2.7**
4.0	**6.3**	**3.6**	**2.8**

Table 3. Uncertainties shown as rms deviations of $\log_{10}A$, related to individual and joint factors

	(1)	(2)	(3)	(4)	(5)	(6)	(7)	(8)	(11)	(12)	S_f	S_{is}	S_{tot}
A	0.047	0.021	0.042	0.066	0.031	0.031	0.028	0.013	0.045	0.024	0.11	0.17	0.21
XL	0.057	0.029	0.072	0.108	0.070	0.041	0.006	0.011	0.038	0.041	0.15	0.18	0.24
L	0.056	0.047	0.058	0.084	0.034	0.037	0.027	0.009	0.045	0.021	0.14	0.22	0.26
M	0.040	0.044	0.025	0.058	0.017	0.023	0.038	0.010	0.045	0.005	0.09	0.18	0.21
S	0.051	0.025	0.030	0.042	0.022	0.025	0.033	0.020	0.041	0.021	0.09	0.14	0.17
a	0.054	0.026	0.047	0.052	0.027	0.031	0.035	0.009	0.057	0.015	0.10	0.14	0.18
v	0.051	0.042	0.064	0.079	0.048	0.041	0.027	0.015	0.053	0.033	0.13	0.12	0.18
d	0.061	0.025	0.068	0.067	0.075	0.038	0.013	0.015	0.045	0.034	0.14	0.18	0.24

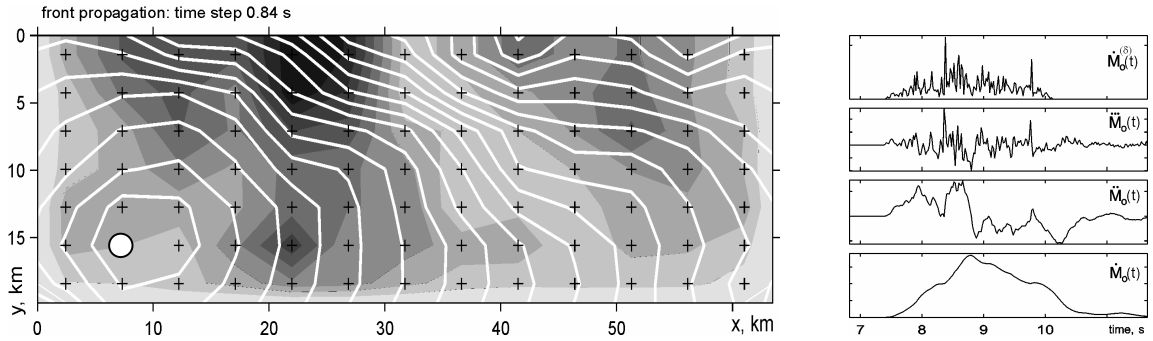

Figure 1: Left: an example of 2D final slip function, shown as shades of grey. Fault parameters: Mw=7.2, L = 63 km, W=20 km. Subsource grid 13×7 (crosses). Random slip follows isotropic k-1.5 wavenumber amplitude spectrum. 2D taper function used over three sides; upper side (y=0) is assumed to cross the Earth surface. White dot is the nucleation point. White contours are successive rupture front positions, simulated kinematically from random rupture velocity field. Right: time histories associated with a particular subsource. The preformed time history is the upper trace. Three other traces are seismic moment time history derivatives $\ddot{M}_0(t)$ $\dot{M}_0(t)$ and $\dot{M}_0(t)$; they represent the subsource contribution to far-field body wave acceleration, velocity and displacement, respectively.

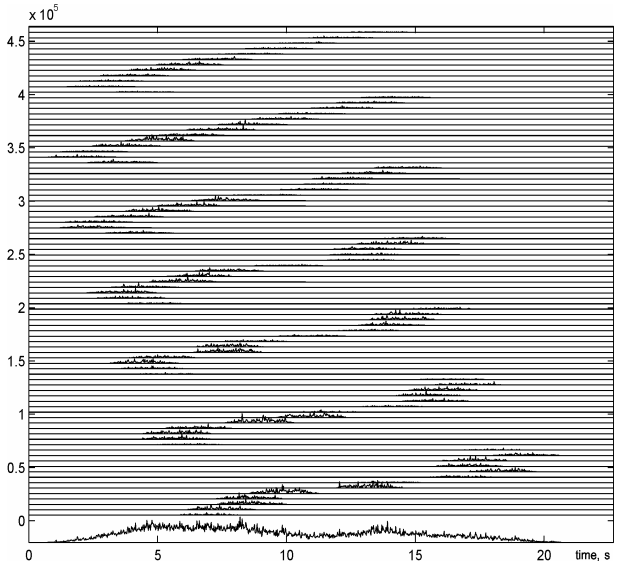

Figure 2: Preformed time histories for 91 subevents of the source of Fig. 1. The lowermost trace is the sum over all subsources.

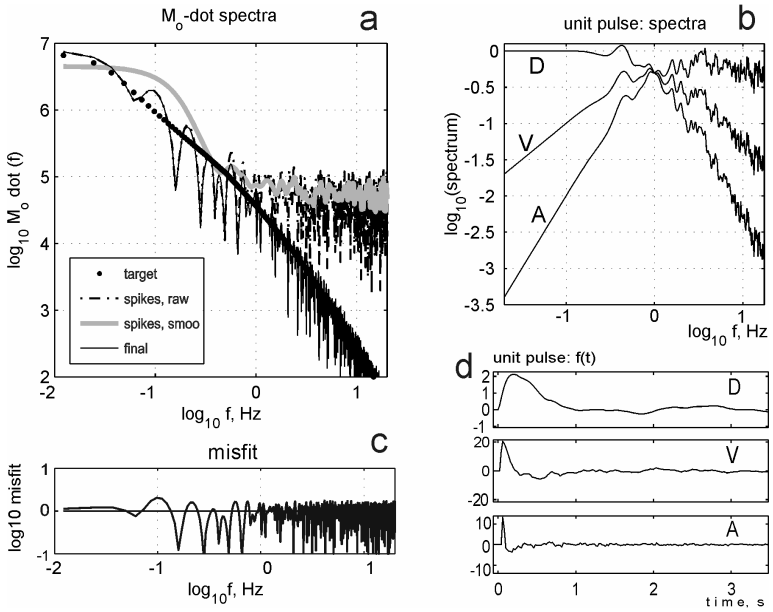

Figure 3: Fitting Fourier source spectra for the discussed example case. *a*: a set of #### spectra (in 10^{20} dyne cm units) that represent: target spectrum, spectrum of the preformed time function (sequence of spikes), its smoothed version, and final spectrum. *b*: Amplitude spectral representation for the "finishing operator" *c*: spectral misfit between target spectrum and final spectrum of graph *a*. *d*: time domain representation of the "finishing operator", or "finishing pulse," (D) and its first and second derivatives (V,A); see graph *b* for corresponding amplitude spectra.

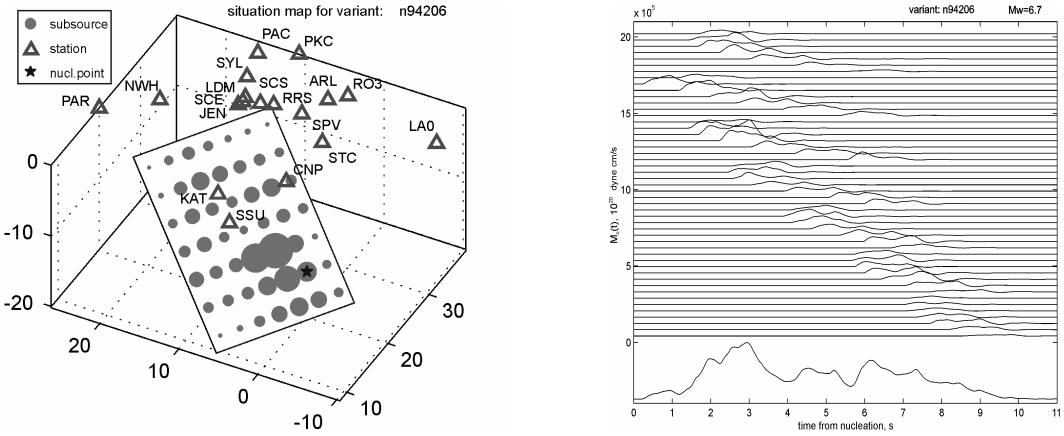

Figure 4. Left: perspective view of source rectangle and receivers/stations for the M_w=6.7 Northridge 1994 event. The subsources are indicated as dots, their size reflects the value of subsource seismic moment as generated for the variant #206. Star is the nucleation point. Coordinates in km. Right: Moment rate time functions for 49 subsources of the variant #206 of a simulated Northridge earthquake; the lowermost trace is their stacked, summary moment rate function.

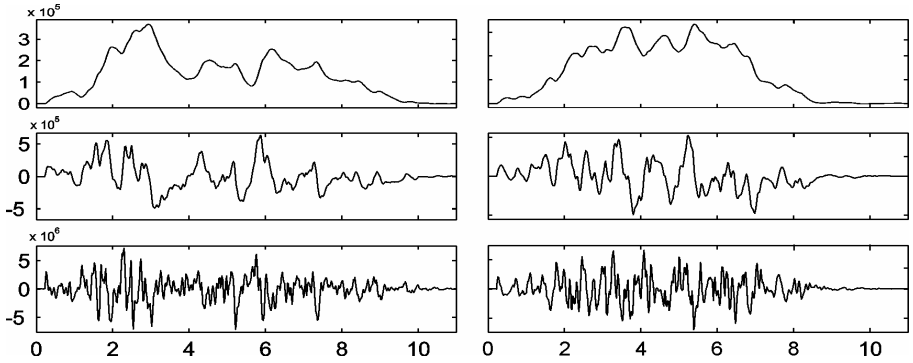

Figure 5. Far-field source time functions for the variants #206 (left) and #300 (right). Top to bottom: functions $\dot{M}_0(t)$ (moment rate), $\ddot{M}_0(t)$, and $\dddot{M}_0(t)$ in 10^{20} dyne cm/s, 10^{20}dyne cm/s^2, and 10^{20}dyne cm/s^3 units.

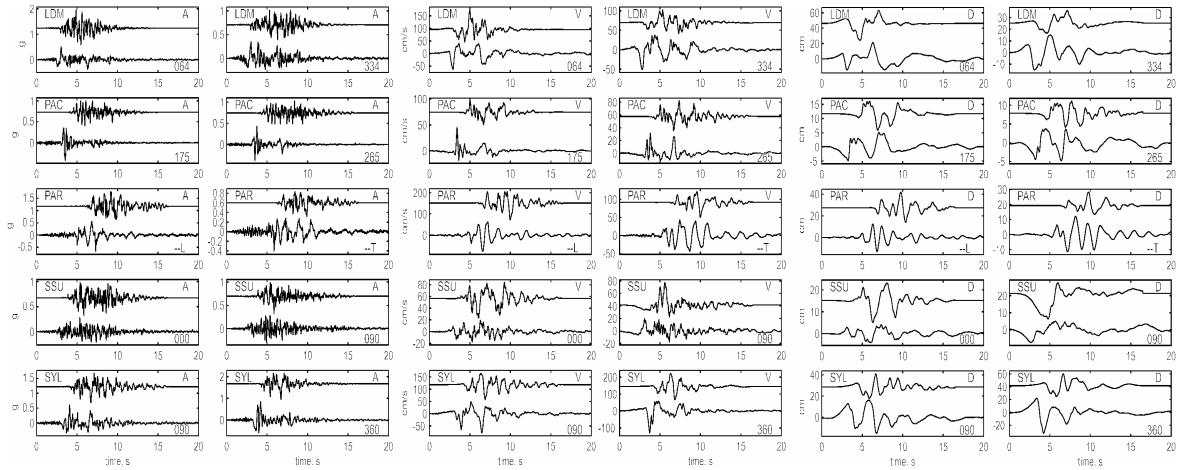

Figure 6. Comparison of observed and simulated (variant #206) time histories for acceleration (left), velocity (center) and displacement (right) for five stations, for two horizontal components. In each box, the lower trace is the observed one and the upper trace is the simulated. Stations, top to bottom, are: PAC, LDM, PAR, SSU and SYL; they are selected at widely different azimuths from epicenter. Ground types are: rock for PAC and LDM, soft rock for SSU and deep soil/basin for PAR and SYL.

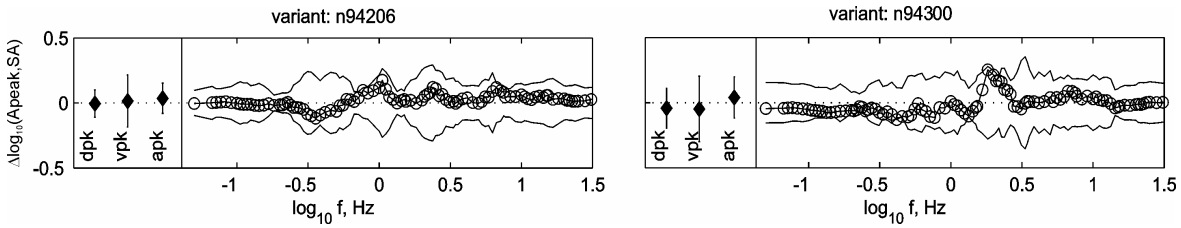

Figure 7. The misfit of horizontal peak and spectral amplitudes over 19 stations, for two simulated variants: #206 and #300. Misfit values are the differences (simulated minus observed) between $\log_{10}$ peak displacements, velocities and accelerations (left box in each graph), and for $\log_{10}$ pseudo response accelerations (right box). All the differences are average values over two horizontal components. Standard deviations over 19 stations for the same data are shown, as error bars for amplitudes, and as a corridor around zero level for spectra.